An optical system to measure the end effector position for on-line control purposes

Theo A. G. Heeren
Frans E. Veldpaus
Department of Mechanical Engineering
Eindhoven University of Technology
NL 5600 MB Eindhoven, The Netherlands

An Optical System to Measure the End Effector Position for On-line Control Purposes

Abstract

This article describes an optical system to measure the coordinates of a manipulator's end effector, which can move in a horizontal plane of approximately 1 × 1 m². Two rotatable laser beams track a retroreflector pair, mounted on the end effector. The coordinates are calculated from the measured beam rotations. The resolution and reproducibility of the coordinate measurement is 0.05 mm. The maximum tracking speed mounts up to 5 m/s. Using components similar to those applied in CD players, the total cost of all mechanical, optical, and analog electronic components can be kept as low as $3000. On an IBM AT-compatible PC, it takes 1 ms to calculate the x *and* y *coordinates from the measured signals.*

1. Introduction

In practical research on the feasibility of controllers for manipulators with flexible links, joints, and transmissions, a principal requirement to compensate for elastic deformations is the measurement of the end-effector position. An indirect approach to this problem is to mount several sensors on the manipulator and to calculate the end-effector's position from the sensor signals, using some manipulator model. Especially when elasticity is involved, this method is unusable, because this model generally is far too inaccurate. In this article an optical system is presented that directly measures the end-effector position and that operates independently of the manipulator. It is intended for manipulators whose end effector can translate in a two-dimensional plane of approximately 1 × 1 m². More detailed information on the system design and its application to on-line control of a flexible manipulator is given by Heeren (1989). The system should satisfy the following requirements:

- The x and y coordinates of a point R on the end effector relative to an orthonormal fixed frame must be measured with a resolution and a reproducibility of 0.05 mm.
- The z coordinate is irrelevant, but the system has to be insensitive to small translations in z direction (less than 3 mm) and to small rotations of the end effector (less than 10°).
- The system must perform well at a maximum end-effector velocity of 5 m/s.
- The measurement must be done in less than 2 ms to enable its application in on-line motion control of the manipulator.
- The system may not impose limitations for the normal operation of the manipulator. No mechanical parts of the measurement system may be located within its working area.
- The cost of the system must be reasonable in relation to the cost of the manipulator.

In view of these requirements, an optical measurement concept has been chosen out of a number of alternatives. It involves the use of semiconductor lasers, rotatable mirrors, retroreflectors, and laser spot detectors. The application of laser interferometry has been discarded because of the high velocity of the end effector and of the severe and expensive quality requirements for the lasers, the system optics, and the electronic circuitry. The chosen principle of operation will be explained in the next paragraph. Then the system design and its parts will be considered more in detail. Finally a calibration procedure will be outlined to extract values for the x and y coordinates from the measurement results once the desired resolution and reproducibility have been obtained.

The International Journal of Robotics Research,
Vol. 11, No. 1, February 1992,

2. Principle of Operation

A schematic top view of the system is given in Figure 1. There are two laser-detector combinations with a flat mirror. The mirrors can rotate about axes in the z direction (perpendicular to the paper) through A and B. Their function is to direct the beams from the semiconductor lasers to the retroreflector pair, attached to point R of the manipulator's end effector, and to redirect the beams, reflected by the retroreflectors, to the duocell detectors. R is the point whose coordinates are to be measured. The retroreflectors deviate an incident beam 180° and shift it in the z direction over a distance that is approximately equal to the distance between the laser and detector centerlines, measured in the z direction. A plano-cylindrical lens (not shown in Fig. 1), mounted in front of the detector, ensures that the beam spot detection is insensitive to small translations of R in the z direction. The duocell detectors measure the position in the x direction of the center of an incident laser beam over a limited range. The rotation angles α_A and α_B of the laser beams are controlled by means of actuators on the mirror spindles such that the distances d_A and d_B between the beams entering and leaving the reflectors, measured in the xy plane, are kept equal to zero as nearly as possible. Under the assumption that all components and their position and orientation in space are ideal, the x and y coordinates (x_r, y_r) of R relative to origin B satisfy the following relations (see Fig. 1):

$$y_r = l - \tan(\alpha_A)\cdot x_r - \frac{d_A}{2\cos(\alpha_A)} \quad (1)$$

$$y_r = \tan(\alpha_B)\cdot x_r + \frac{d_B}{2\cos(\alpha_B)} \quad (2)$$

Hence x_r and y_r can be calculated if d_A, d_B and the mirror rotation angles $\alpha_A/2$, $\alpha_B/2$ are measured. In Section 9 the influences of component deficiencies and of errors in their positions and orientations are considered.

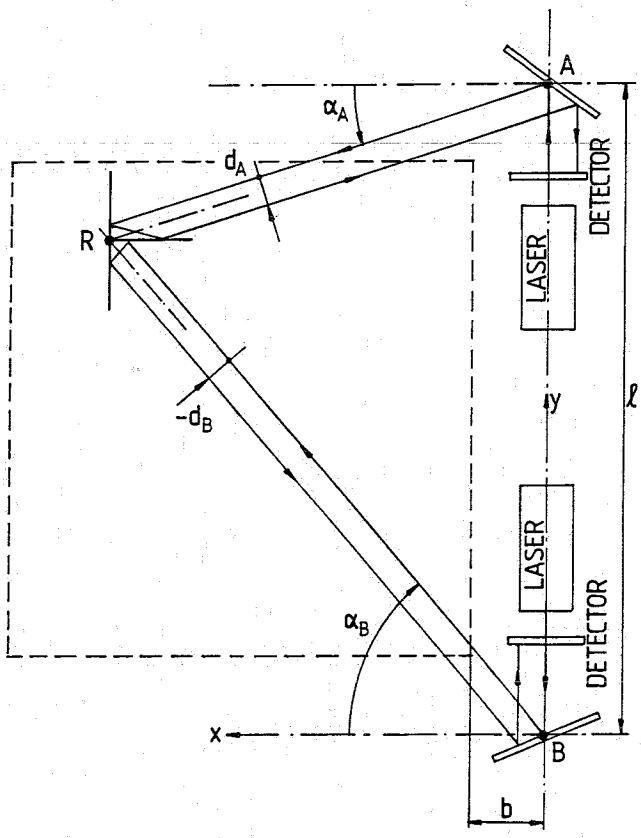

Fig. 1. Schematic top view of the system.

3. The Lasers

A laser beam and its propagation in space can be described with several characteristics (Melles Griot 1988). Because we do not work with laser interferometry, we are not interested in a large coherence length or a perfect plane wavefront of the laser beam. Characteristics like wavelength, beam diameter, angular drift of the beam centerline, and divergence are more important in our case. Figure 2 illustrates the propagation of a laser beam in space. The divergence θ occurs as a result of diffraction of light passing through an aperture. In the direct neighborhood of the aperture, the diameter equals the diameter d_0 of the aperture. At a distance p, much larger than d_0, the beam diameter asymptotically approaches the product of divergence θ and propagation length p. From fundamental optical principles, it follows that divergence is inversely proportional to d_0.

A semiconductor laser of type CQL30 or CQL16 (Philips Collimator Pen) turned out to be suitable for our purpose. The beam divergence θ is approximately 0.3 mrad for a diameter of 5.4 mm and a wavelength of 780 nm. The laser beam is first guided through a circular hole of 2.5-mm diameter, so the divergence will increase to approximately 0.6 mrad.

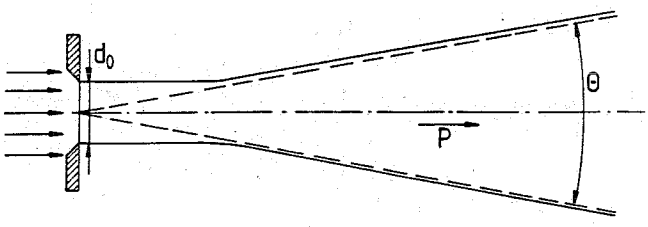

Fig. 2. Laser beam propagation.

This reduction of the beam diameter is introduced in order to minimize the size of all mirror surfaces in the system. This size is mainly determined by the magnitude of the elliptical projections of the round beam on the plane mirror surfaces. The total beam length from the laser to the corresponding detector can vary from 0.5 to 4 m in our system. Within this range the beam diameter should be kept as constant as possible in order to enable a well-conditioned measurement of the beam centerline position by the duocell detector. At a propagation length of 4 m, the beam will have a diameter of 2.5 mm ($\approx$4 m $\times$ 0.6 mrad), which is equal to the hole diameter. Thus it is reasonable to assume that in the interval from 0.5 to 4 m the beam will have an approximately constant diameter of 2.5 mm. The diameter cannot be reduced any further, because the divergence would then become too large.

If the laser operates stationarily, the angular drift of the laser beam centerline can be neglected. The static angle between the optical and mechanical axis is smaller than 10 mrad for our laser type. This static misalignment can, to a certain extent, be eliminated by adjusting the laser holder.

The maximum output power of the laser beam is 2 mW, resulting in a maximum average illuminance of 12.3 mW/cm^2 behind the circular hole (to calculate the illuminance, the Gaussian distribution of the illuminance must be taken into account). This is large enough to provide good measurement conditions at the duocell detectors. The laser is connected to an electronic circuit to control the laser beam power in the range from 0 to 2 mW. The circuit keeps the laser beam power, which is measured by a photodiode in the collimator pen, at a desired level.

4. The Retroreflectors

A retroreflector consists of three mutually orthogonal, flat mirrors with one common point R. Ideal retroreflectors have the properties that, regardless of the reflector orientation, an incident beam and the reflected beam are parallel and that the corner point R is always exactly in the middle between the incident and the reflected beam. These properties are

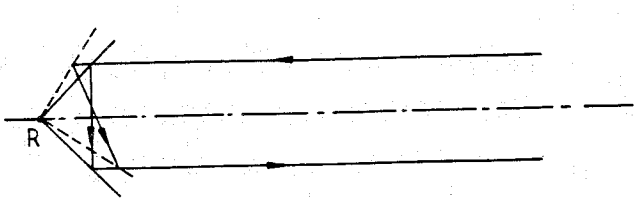

Fig. 3. Retroreflector principle.

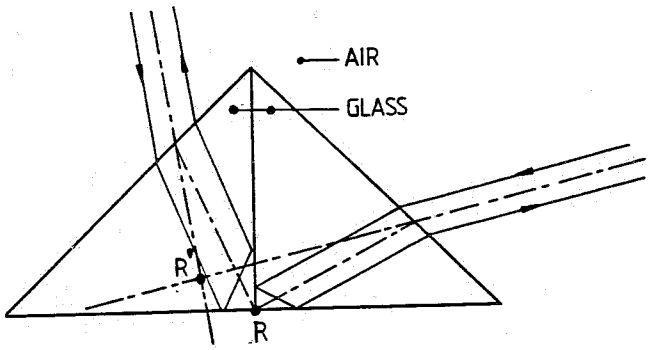

Fig. 4. Solid glass reflectors.

shown in Figure 3 for the two-dimensional case, but also hold for the three-dimensional case. The second property is not applicable to solid glass retroreflectors (also called *corner cubes*) because of refractions at the entrance/exit face, as shown in Figure 4. Because the angular orientation of the reflectors, attached to the end effector, is not precisely known, there is no way of compensating for the difference between R and R′. Therefore solid glass reflectors cannot be used for our purpose. In order to make the corner points of both reflectors coincide with one point R on the end effector, we use a metallic mirror reflector consisting of two triangular prisms mounted on a flat mirror, as shown in Figure 5. It should be avoided that laser beams are reflected at any of the edges of a reflector mirror. This could cause distortions of the beam, because the edges are beveled. Under normal operation the distance between the incident and the reflected beam, measured in the z direction, lies in the range from 9 to 17 mm. Under this circumstance there is no reflection at any of the edges for a sufficiently large range of angles of incidence.

The assembly of the reflector pair has to be carried out very accurately; to assure a sufficiently large orientation independence of the reflected beam, the angle between the incident and the reflected beam should be equal to $180° \pm 6.10^{-4°}$. The reflector pair is made of glass with a gold coating on all reflecting surfaces. This results in a 95%

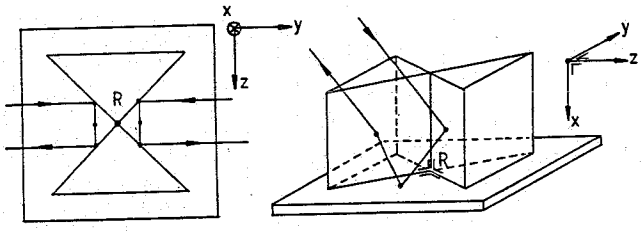

Fig. 5. Double reflector structure.

reflectance in the infrared area (wavelengths above 700 nm).

A laser beam that is directed at a mirror can be seen as the superposition of two plane-polarized beams, one parallel to the plane of incidence (p-polarized) and one perpendicular to the plane of incidence (s-polarized). For mirrors with a metallic reflecting surface, the reflectances of the p and s components of the beam are not equal and depend on the angle of incidence. Therefore the intensity distributions of the p and s components of the laser beam have to be such that no shift of the centerline of the beam occurs if the angle of incidence changes. From Figure 1 it can be seen that each laser beam is reflected five times by a metallic mirror before it hits a detector, so it is important to consider this phenomenon.

Mirror reflectance rapidly decreases as the angle of incidence of the beam relative to the mirror plane becomes smaller than 12°. Moreover, the size of the reflectors must be kept within reasonable proportions; no mirror plane should be larger than 50 mm in any direction. This means that the angles of incidence of the laser beams relative to the reflector mirror planes have to be bounded and that α_A and α_B should be kept between 12° and 78°.

5. The Plano-Cylindrical Lens

As stated before, the maximum allowable translation of the end-effector point R in the z direction is 3 mm upward and downward. Hence the distance between the incident and reflected beams can vary over a range twice as large (i.e., 6 mm upward and downward). This is liable to lead to detection problems, because the height of the photosensitive area of the detector is only 2.5 mm. Thus the beam has to be focused in the detector range without affecting the beam centerline shift in the x direction that is to be measured by the detector. This can be realized by putting a plano-cylindrical lens in front of the detector with its focal axis perpendicular to the z direction, as shown in Figure 6. If the detector is placed at the focal axis of the lens, the detector area will see a very thin and bright stripe with a length of 2.5 mm. If the illuminance at the focal axis is too large for the detector's photo-sensitive material, the detector can be placed a little before or behind the focal axis. Then the detector sees a narrow ellipse that can translate a little in the z direction, but never outside the detector range.

6. The Duocell Detector and its Electronic Circuitry

A duocell detector consists of two photodiodes with adjacent radiant sensitive areas, as shown in Figure 7. It can be used to measure the centerline position in one direction only of an incident laser beam (denoted by the dotted lines) of appropriate wavelength, provided that the beam diameter and the measurement range are not too large in relation to the radiant-sensitive areas. A detector that is suitable for our purpose is the SPOT-2D detector (United Detector Technology). The radiant sensitive areas are each 1.25 × 2.5 mm large and they are spaced 100 μm apart. Thus the laser beam with a diameter of 2.5 mm is of the same order of magnitude as the detector areas, and the beam centerline can easily be detected as far as the dimensions are concerned.

Under the condition that the reverse voltage over the diodes is kept equal to zero, it follows from the detector characteristics that each of the diodes outputs a current, the so-called photocurrent, which is proportional to the power of the light falling on the radiant-sensitive area of the diode. The current through the diode, if there is no illumination at all, is called the *dark current*. Thus the total photocurrent consists of the dark current and the current resulting from detector illumination. The dark current can be seen as an undesirable bias and must be kept as small as possible in relation to the illumination current. The detector characteristics show that the dark current increases as the reverse voltage over the diode increases. Hence the illumination current is made as large as possible by choosing the laser

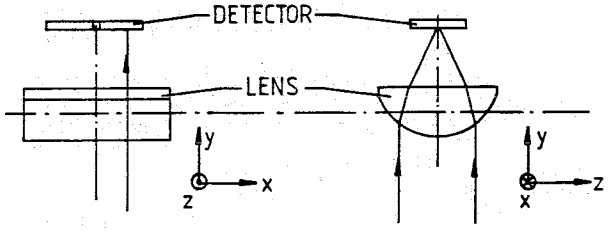

Fig. 6. Plano-cylindrical lens principle.

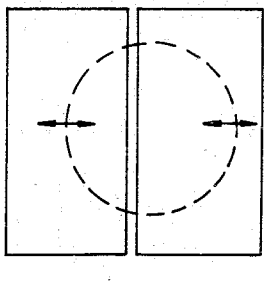

Fig. 7. Duocell detector.

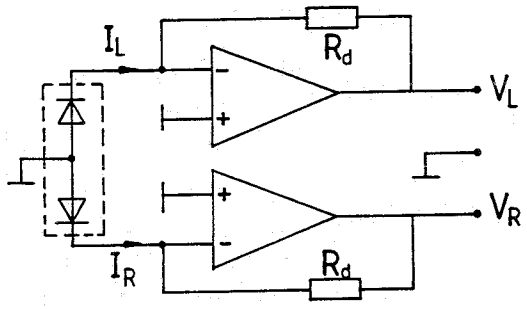

Fig. 8. Duocell detector circuit.

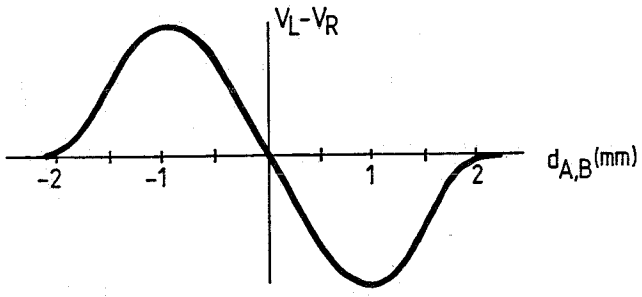

Fig. 9. Differential voltage versus beam position.

beam illuminance as large as the diode can sustain, and the dark current is made as small as possible by keeping the voltage over the diodes equal to zero. This can be achieved using the electronic circuit shown in Figure 8, which transforms the photocurrents I_L and I_R into the voltages V_L and V_R, respectively. In spite of the fact that the internal diode capacitance grows with decreasing reverse voltage, the bandwidth of the transfer functions from laser beam illuminances to the output voltages of the circuit is larger than 10 kHz, which is high enough for our application. From the duocell characteristics, it follows that at a reverse voltage of 0 V, the dark current remains below 5 nA. To calculate the photocurrent resulting from laser beam illumination, the power of the beam at the detector surface must be known. Departing from the laser at an illuminance of 123 W/m^2, the beam is reflected five times with approximately 5% loss of illuminance at each mirror reflection (see Fig. 1). Then it passes through the plano-cylindrical lens, causing another 5% loss of illuminance. So the beam with a diameter of 2.5 mm arrives at the detector surface with a power of 0.445 mW ($= \pi/4.(0.0025)^2.123.(0.95)^6$). The photocurrent resulting from beam illumination can be calculated by multiplying the incident light power by the sensitivity of the radiant sensitive material, which equals 0.38 A/W at the wavelength of 780 nm. If we assume that 40% of the beam power actually hits each of the two photodiodes, this results in a photocurrent of 67 μA per diode. Thus the illumination current is at least 10.000 times larger than the dark current if the laser beam is centered in the middle of the detector. This ratio is large enough to use the output voltages V_L and V_R for control of the mirror rotations. If we want a current of 100 μA to correspond with an output voltage of 10 V, we have to choose R_d in Figure 8 equal to 100 kΩ. The two resistors must be equal. Additional trimming potentiometers may be necessary to realize this. The input current of the operational amplifiers in Figure 8 must be very small in comparison with the photocurrent. For this purpose MOSFET operational amplifiers (opamps) with an input current smaller than 1 nA are suitable (Burr Brown Corporation 1987). If the beam is in the detector range, the output voltage difference $V_L - V_R$ depends on the beam position on the detector surface, as shown in Figure 9. At the detector centerline, the positional sensitivity can be set at 10 V per mm beam displacement by choosing the appropriate value of R_d. With a signal-to-noise ratio of 2000 beam displacements of 500 nm can be detected.

A final design aspect is the minimization of the disturbing effect of ambient daylight shining on the detector. This can be done by creating a dark surrounding for the detector with apertures just large enough for the laser beams to pass through. If this turns out to be not satisfactory, a filter can be mounted in front of the detector that transmits infrared light (wavelength > 700 nm) only. In our design the photocurrent resulting from daylight illumination mounted up to 40 nA for each diode. Because the daylight did not have a significant influence on the difference between the currents, the filters have been discarded.

7. Design of the Rotatable Mirror and its Actuator

The measurement system requirements concerning the position range, the maximum speed, and the maximum acceleration of the manipulator's end effector lead to a set of requirements for the rotatable mirrors, their actuators, and the electronic mirror control circuitry. The mirror rotations must be controlled such that the laser beams follow the reflector pair. First of all, the positions of the mirror rotation axes relative to the measurement area of approximately 1 × 1 m^2 have to be determined. These positions are characterized by l and b (see Fig. 1). The highest possible resolution is obtained by mounting the mirrors as closely as possible to the measurement range, because then a certain displacement of the retroreflector pair in the xy plane leads

to the largest possible rotations of the mirrors. On the other hand the proper operation of a retroreflector requires that α_A and α_B (see Fig. 1) stay between 12° and 78°. A final aspect to be taken into consideration is that in the neighborhood of the line *AB*, measurement conditions are very bad because of the fact that α_A and α_B hardly change as a function of reflector pair displacement in the *y* direction. It then turns out that *l* should be at least 1.7 m and *b* at least 0.3 m. If the maximum speed of the end effector is 5 m/s and the maximum acceleration is 100 m/s^2, the maximum angular speed of the mirrors equals 5 rad/s and the maximum acceleration is 125 rad/s^2. These values correspond to the case where the end effector is positioned in the corner of the measurement area as closely as possible to a mirror. This is a worst case that will never occur at maximum speed. It is noted that the mirror speed and acceleration are twice as small as the speed and acceleration of the laser beams.

The rotation of the mirrors must be adjusted very accurately in order to obtain the desired resolution and reproducibility. Thus the mechanical design of the rotatable mirror and its actuator must provide the possibility for fine adjustment, and the position of all mechanical components must be reproducible. Phenomena like Coulomb friction and clearances have to be avoided to make this possible. This has led to a scanner design consisting of a closed box (with an aperture for the laser beams to pass through) that contains the rotatable mirror structure and an adjustable laser detector unit. The box is placed on a platform that is made adjustable in all six degrees of freedom, so that the plane in which the laser beam rotates can be aligned to the plane in which the reflector pair can move. The laser detector unit in the box is also made adjustable in order to align the laser beam centerline to the rotation axis of the mirror. Flexural pivot bearings (Bendix 5004-800) have been used to support the mirror spindle. These bearings consist of blade springs and therefore have a limited rotation range of only 40°. This, however, is no problem, because the desired rotation range of a mirror equals 33° (= [78° − 12°]/2). Flexural pivot bearings have advantages that make them superior to other types of bearings in our application, as they show no Coulomb friction and no clearance, which enables accurate mirror positioning. Another important property is that their radial displacement (which is smaller than 5 μm) is a reproducible function of the rotation of the mirror. Moreover, the radial displacement of the upper flexural pivot will be equal to the displacement of the lower flexural pivot. Hence the mirror rotation axis will keep pointing in the *z* direction as the rotation of the mirror varies. Hence the surface in which the laser beam moves as the mirror rotates then will be as plain as possible, and alignment problems will be minimized. The applied flexural pivot bearings behave like torsion springs with an approximately constant stiffness equal to $1{,}28.10^{-3}$ N·m/rad per bearing.

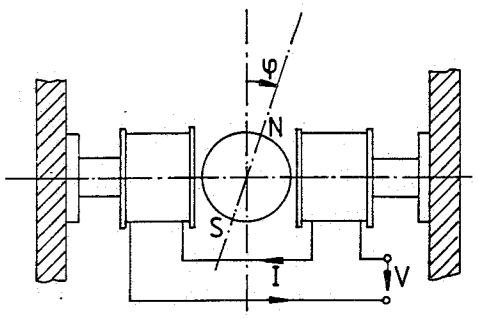

Fig. 10. The actuator.

The actuator consists of a round permanent magnet (samarium cobalt, 1 T) mounted on the mirror spindle and two coils with adjustable ferroxcube cores attached to the walls of the box, as shown in Figure 10. The small rotation range of the mirror enbles this brushless design, thus eliminating Coulomb friction and preserving positioning accuracy. The electrical part of the actuator can be modeled as follows:

$$L\dot{I} + R_c I + K\dot{\varphi} = V. \tag{3}$$

Here *I* is the current through the coils, *V* the voltage over both coils, φ the mirror angle, *L* the self-inductivity, R_c the coil resistance, and *K* the torque coefficient. The torque coefficient is nearly independent of the mirror angle within the relevant rotation range and is equal to $6{,}2.10^{-3}$ N·m/A, the resistance R_c equals 27,5 Ω, and the self-inductivity *L* is 8,3 mH. These data have been determined experimentally (van Driel 1988). If the actuator current is zero, there is still a nonzero torque acting on the spindle because of the interaction between the permanent magnet and the ferroxcube cores. This torque is experimentally determined as a function of the mirror rotation, depicted in Figure 11. The amplitude of this curve can be modified by changing the distance between the ferroxcube cores in the coils and the permanent magnet. Moving the cores of course also influences the values of *K* and *L*, but this variation is limited to 20%. It follows from Figure 11 that within the actuator range, denoted by the dotted lines, the magnetic stiffness K_M is approximately constant and negative (order of magnitude, -2.10^{-3}

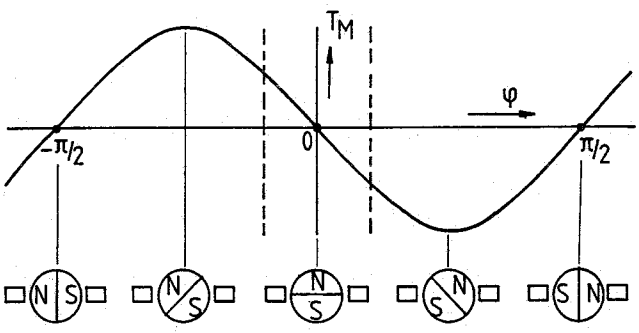

Fig. 11. Permanent magnetic spring characteristic.

N·m/rad). The mechanical part of the actuator can now be modeled with one degree of freedom φ:

$$J\ddot{\varphi} + d\dot{\varphi} + (K_B + K_M)\varphi = KI. \qquad (4)$$

Here J is the moment of inertia of all rotating parts (10 g·cm^2), d is a damping coefficient that accounts for the low hysteresis of the bearings, and K_B is the torsion spring stiffness of both bearings (2,56.10^{-3} N·m/rad). In the experimental setup, it turned out to be possible to partially compensate the positive stiffness of the flexural pivot bearings by means of the negative stiffness caused by the interaction between the permanent magnet and the ferroxcube cores. The cores can be positioned in such a way that the resulting stiffness $K_B + K_M$ is a little larger than zero (for the sake of stability in combination with the electronic control circuit). The stiffness compensation has two major advantages: (1) the current through the coils can be made considerably smaller, because the flexural pivot spring torque does not have to be compensated by the electromagnetic actuator torque KI; and (2) the mirror rotation can be controlled more accurately by a simple analog PD controller, because the static tracking error (in the distance from the laser beam centerline to the detector centerline, d_A or d_B in Fig. 1) will be smaller because of the fact that the resulting spring stiffness is smaller. The inclusion of integral action in the controller then becomes superfluous.

The current through the coils is supplied by an analog current amplifier that keeps the current proportional to an amplifier input voltage coming from the control circuit. The bandwidth of the transfer function from the input voltage to the actuator current is 22 kHz, which is high enough in relation to the location of the poles of the transfer function from the current to the mirror rotation angle to assume a static relationship between the input voltage and the actuator current.

The actuator has to be capable of supplying the highest peak torque required by the rotatable mirror in order to perform well. A second actuator design criterion is that the continuous dissipation power in the actuator coils remains below 100 mW per coil in order to prevent the coils from heating up. If we assume that the bearing hysteresis is negligibly small, then it follows from eq. (4) that the actuator torque KI will be used to compensate the resulting spring torque (estimated stiffness $K_B + K_M$ = 0,4.10^{-3} N·m/rad) and to accelerate the mirror and all mechanical parts attached to it (moment of inertia J: 1.10^{-7} kg·m^2). So the maximum torque required by the mirror in order to follow the retroreflector's movements can be calculated as follows:

$$\begin{aligned} T_{max} &= J\cdot\ddot{\varphi}_{max} + (K_B + K_M)\cdot\varphi_{max} \\ &= 0{,}125.10^{-3} + 0{,}119.10^{-3} \\ &= 0{,}244.10^{-3}\ \text{N·m} \end{aligned} \qquad (5)$$

This corresponds to an actuator current of 40 mA ($= T_{max}/K$). This value is quite acceptable, as it leads to a maximum dissipation of 22 mW per coil.

The mirror will not always operate in the normal following mode (the mode in which the mirror tracks the retroreflector). We have to take into account the possibility that the laser beam can be interrupted by some disturbing object in the measurement area. If that happens, the mirror rotation can no longer be controlled in such a way that the laser beam keeps track of the reflector, and the laser beam will be reflected outside the range of the duocell detector. The mirror control circuit can detect this, since the sum of the two photocurrents coming from the diodes of the detector then decreases below an admissible level. This condition makes the control circuit select the scanning mode. This is a mode in which the mirror slowly moves up and down in its whole range, with the objective to regain laser beam contact with the retroreflector. As soon as this happens, the sum of the detector currents will rise to a normal level, and the control circuit switches on the PD controller again (back to following mode). The scanning mode is also used to provide a proper system start-up. A schematic view of the mirror control circuit is given in Figure 12. The inputs are the two voltages V_L and V_R, proportional to the photocurrents of the detector. The difference and the sum of V_L and V_R are determined. The difference is led into a PD controller (for the following mode), whose output goes to a multiplexer. For the scanning mode, a triangular signal coming from a tunable generator is also led to the multiplexer. The sum of the input voltages is Schmidt triggered (with a tunable level) and then used to make the multiplexer switch between the PD controller or the generator signal.

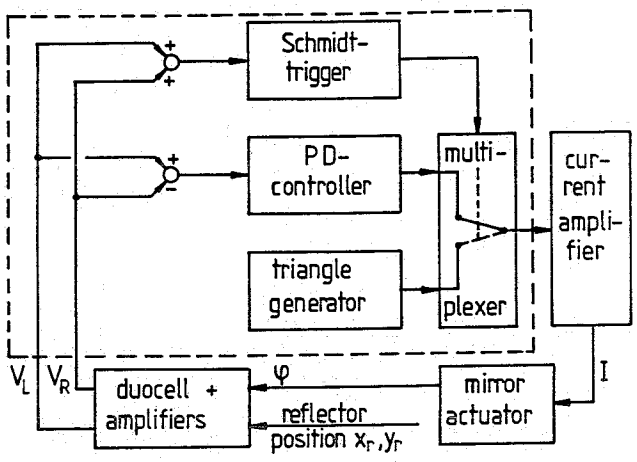

Fig. 12. The mirror control circuit.

The output of the multiplexer goes to the current amplifier that is connected to the mirror actuator. The PD controller has to satisfy two design criteria. First, it has to make the laser beam track the reflector once the laser beam is in the detector range by keeping the difference between the input voltages as small as possible. Second, it must be capable of "catching" the laser beam on the detector surface in case the control circuit switches from scanning mode to following mode. This is the more critical criterion. At a scanning speed of 0.6 rad/s, the laser beam sweeps over the detector surface with a speed of at most 2.5 m/s. The PD controller is active within a range of 2 mm of the detector range, so the time available to decelerate the mirror speed from 0.6 rad/s to zero is a little above 0.5 ms. This requires a peak deceleration of 1200 rad/s^2, corresponding to a peak current of 200 mA. The bandwidth of the current amplifier must be high enough to supply this current within 50 μs. A final aspect to be taken into account in the design of the mirror controller is that if a PD controller with a constant proportional and differential action is used, as in our case, the gain of the feedback loop is proportional to the length of the laser beam that can vary from 0.5 to 4 meters. For given reflector coordinates x_r, y_r the desired mirror angle φ_d, for which the differential voltage $V_L - V_R$ (a measure for either d_A or d_B; see Fig. 9) is zero, can be calculated. The tuning of the PD controller is carried out such that the bandwidth of the transfer function from φ_d to φ is as large as possible, while the controlled system remains stable and the catching operation succeeds everywhere in the measurement area. For a point in the middle of this area, the bandwidth is approximately 600 Hz. However, if the calculation of x_r and y_r is based on measurement of α_A, α_B, d_A, and d_B (for instance in eqs. [1] and [2]), the dynamic behavior of the mirror is irrelevant as long as the laser beams remain within the detector range. The bandwidth of the duocell detectors and their electronic circuitry that measure α_A, α_B, d_A, and d_B is approximately 10 kHz. The total time delay in the determination of x_r and y_r is influenced by this bandwidth and by the processing time to calculate x_r and y_r. We will return to this subject in section 9.

8. Measurement of the Mirror Rotation Angle

To obtain the desired measurement accuracy of 0.05 millimeters in the end-effector position, the rotations of both mirrors must be measured with a resolution and a reproducibility of 10^{-5} rad or better. From a number of alternatives, optical encoders have been chosen. The encoder consists of a code wheel (Hewlett Packard HEDS 6100) with 1000 slits, mounted on the mirror spindle, and a set of encoder modules built around it, according to Figure 13. Module 3 is a HEDS 9000 incremental encoder module (Hewlett Packard). It contains opto-electronic circuitry to monitor the code wheel slits. There are two detectors in this module that are spaced apart over a quarter of a code wheel cycle (i.e., the angle between two subsequent code wheel slits). The detector signals (called *A* and *B*) are triggered so distinction is only made on the level of dark and light. They are functions of the code wheel position, as depicted in Figure 14. There are four transitions from light to dark and vice versa in one code wheel cycle. The signals are led to a quadrature decoder/counter interface (Hewlett Packard HCTL 2000) that contains a 12-bit up/down counter register whose value is a measure for the rotation of the code wheel in units of a quarter of a code wheel cycle ($= 2\pi/4000 = 1.57$ mrad). The interface can detect the direction in which the code wheel rotates from the

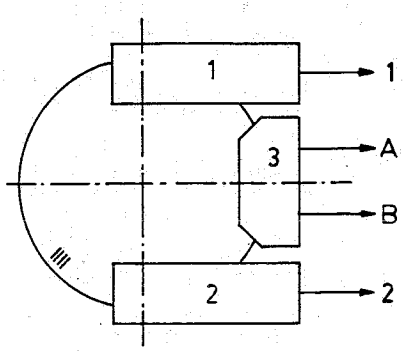

Fig. 13. The code wheel with the encoder modules.

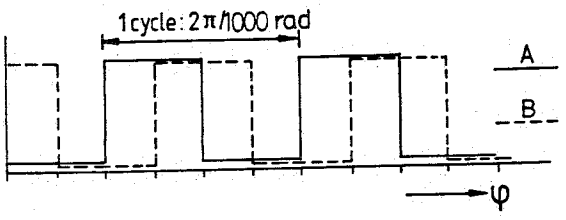

Fig. 14. Signals from the HEDS 9000 module.

order in which the transitions on the signals A and B occur. The resolution of 1.57 mrad is not accurate enough for our purpose. This is the reason the additional encoder modules 1 and 2 are built around the code wheel. Each of these modules consists of a light source on one side of the code wheel and a duocell detector on the other side. This detector produces an approximately sinusoidal signal (i.e., the difference of the two photocurrents) for each code wheel cycle. Modules 1 and 2 are placed such that their signals are also shifted a quarter of a cycle. In Figure 15 they are given as a function of the rotation φ. In the intervals 1 and 3, denoted in Figure 15, signal 1 is a well-conditioned measure for the mirror rotation angle, whereas signal 2 shows extrema in these areas and is thus ill conditioned. In areas 2 and 4, it is the other way around: signal 2 is well conditioned here. Encoder module 3 is placed in such a way that the value of the 12-bit up/down counter register indicates the current interval. The signals 1 and 2 are sampled and then digitized by means of a 12-bit A/D converter. The counter and conversion values are then processed by a microprocessor to determine the mirror rotation angle.

The procedure just described will only work correctly if the signal-to-noise ratio of the signals 1 and 2 is large enough to measure the mirror rotation with a resolution of 10^{-5} rad and if these signals show a reproducibility of at least 10^{-5} rad, meaning that if the same mirror rotation is measured at two arbitrary moments, the difference in measurement results may not correspond to a rotation difference larger than 10^{-5} rad. From the experimental results it follows that the signal-to-noise ratio of the signals coming from the modules is larger than 2000, so the most significant 10 bits of the 12-bit A/D conversion results can be trusted, whereas only the first eight bits are needed in order to obtain the desired resolution. Some more effort is required to obtain the desired reproducibility. The most important source of a bad reproducibility is the fact that the sensitivity of the photosensitive material of the detectors can easily vary a few percent as the surrounding temperature changes a few degrees. Moreover, the light source on the other side of the code wheel does not emit a constant light power if it is connected to a voltage source. The light power varies as a function of temperature. We can circumvent these problems by designing the encoder module according to the scheme in Figure 16. The light, emitted by an infrared Light Emitting Diode (LED), falls through a code wheel slit, then through a slit attached to the module, and finally hits the radiant-sensitive areas of the duocell detector. The position of the center of the light beam falling on the detector is then a measure for the code wheel rotation. Reproducibility of the difference between the photocurrents coming from the detector is now improved by connecting the LED to an electronic control circuit that keeps the sum of the two photocurrents equal to some adjustable, constant value. In this way the influence of temperature on the illuminance of the LED and on the sensitivity of the duocell detector are compensated via the optical feedback. Moreover, the variance of almost 40% in code wheel slit width is partially compensated: if a wide slit passes between the LED and the detector, the LED power will be smaller, and if a narrow slit passes by, the LED power will be larger in order to keep the total amount of light falling on the detector constant. It is assumed that the temperature dependence of the sensitivity is equal for both diodes of the duocell detector. The difference between the photocurrents has now become a reproducible measure for the code wheel rotation within one code wheel cycle.

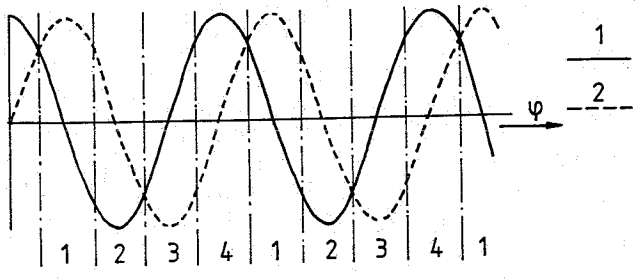

Fig. 15. Signals from the additional modules.

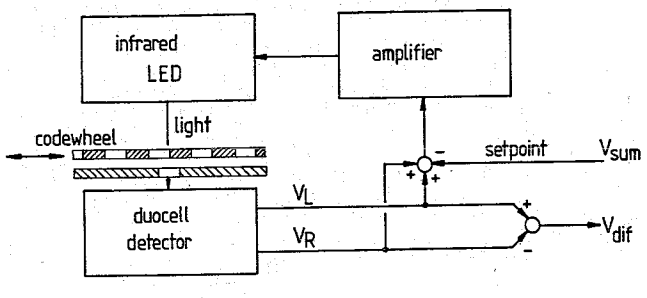

Fig. 16. Design of the encoder module.

9. The Calibration Procedure

After obtaining a satisfactory resolution and reproducibility of the measurement system, the calibration of the system is the final step in order to achieve absolute measurement accuracy (i.e., the determination of the coordinates x_r and y_r of the point R on the end effector). For several reasons it is undesirable to simply calculate these coordinates using formulas (1) and (2). First of all the lasers, detectors, and mirrors do not have the ideal position and orientation in space. Even though most of these components are mounted in adjustable holders, it is practically impossible to determine whether a component is ideally positioned. The adjustment possibilities are mainly used to make the system operate correctly (i.e., the catching and tracking of the reflector pair in the whole measurement range). Very small misalignments would lead to differences in measurement results relative to eqs. (1) and (2) of several tenths of millimeters. Second, the profiles of the signals coming from the encoder modules are not exactly known as a function of code wheel rotation. (They look like sines.) Moreover, they can be slightly different for each code wheel slit. In order to find a relationship between the signals from the measurement system and the coordinates x_r, y_r, we need a second measurement system exclusively for the calibration. This second system must deliver the coordinates of a large set of calibration points on the boundaries of the measurement area, as shown in Figure 17. These calibration points have been chosen as far away as possible from the scanner that is being calibrated in order to obtain maximum measurement accuracy within the measurement area. The accuracy of the calibration measurement system must at least be better than 0.05 mm, which is the accuracy of the measurement system that is calibrated. It is advisable to choose four or more calibration points per code wheel slit, as the encoder module signals can be slightly different for each code wheel slit. If it is assumed that the position measurement of each calibration point is performed in a static manner, then a possible static tracking error in the mirror rotation can also be measured and compensated. If 1000 calibration points per scanner are used, the calibration data can be put in a table that occupies 20 kilobytes of computer memory.

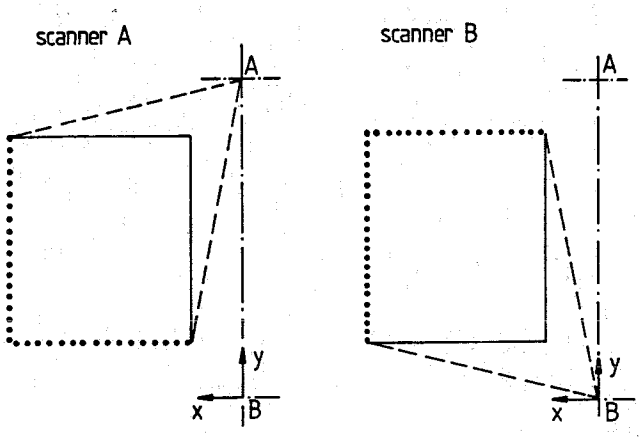

Fig. 17. Calibration points.

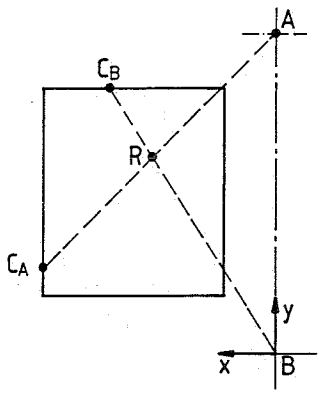

Fig. 18. Coordinate determination.

In order to determine the coordinates x_r and y_r of the point R on-line, the microcomputer, which monitors all signals of the measurement system, first has to acquire the counter values of the HCTL 2000 decoder/counter interfaces and the digitized values of the signals from the additional encoder modules and from the tracking error signals of both mirrors. Then for each scanner, the x and y coordinates of the point on the boundary of the measurement area at which the laser beam is pointing are determined via interpolation between the calibration point values, resulting in the coordinates of the points C_A and C_B in Figure 18. Under static conditions, the x and y coordinates of the point R on the end effector can be calculated as the intersection point of the two lines shown in Figure 18. Under dynamic circumstances it is possible to compensate the tracking errors of the mirror control circuits using the measured values that determine d_A and d_B. This can be done by adding 50% of these distances to the intersection point position in directions perpendicular to the lines AR and BR, respectively (see Figs. 1 and 18). In the experimental setup it turned out that an IBM AT-compatible personal computer running at 6.5 MHz can carry out all these tasks in 1.1 ms.

10. Conclusion

The measurement system described in the previous paragraphs turned out to work satisfactorily under the laboratory conditions for which it was designed and tested. However, it is questionable whether it is also suitable for more rigorous factory conditions. After all, the chosen measurement concept is not very robust; as long as the laser beams are interrupted, the system simply does not work. It is quite probable that an object that is held by a manipulator's end effector causes laser beam interruption. On the other hand, it must be stated that hardly any other measurement concept (nonoptical) can be found that is capable of measuring the end-effector position directly. Perhaps the robustness can be improved by working with more than two laser detector combinations. It may also be possible to discard the retroreflectors by mounting the detectors directly on the end effector using lenses with a wide-angle view. Retroreflectors are sensitive to scratches and dust, so it is advisable not to use them under factory conditions.

The cost of the measurement system components mounted up to $3000, which is very reasonable in relation to the cost of the manipulator for which it was used. This shows that as far as the measurement system is concerned, a flexible, light manipulator design in combination with a measurement system like the one presented here may be economically compatible with the usual manipulator design: stiff structures that are controlled via servomotor position feedback.

The calibration procedure using the second measurement system has not been carried out in our case. The objective of this research was to produce a measurement system with the desired resolution and reproducibility of 0.05 mm, not a system that offers absolute measurement accuracy. Absolute measurement accuracy is not required in order to perform research on controller feasibility for flexible manipulators using end-effector position feedback. The servomotor positions of the manipulator for which the measurement system was designed were used as calibration values, rather than measuring the values by means of a second measurement system.

In principle the measurement concept presented here is also suitable for a 3D measurement system. Instead of duocell detectors, quadrant detectors would then have to be used to measure the laser beam spot location in two directions. The mirror would have to be made rotatable about two axes, or two separate mirrors rotatable about one axis would have to be used in order to direct the laser beam at the reflector. If the laser beam is interrupted, it would cost considerably more effort and money to let the laser beam regain contact with the reflector; a three-dimensional space cannot be scanned as simply as can be done in a two-dimensional plane. Moreover, it will be more difficult to measure the mirror positions. Fast digital image processing would then become more appropriate. At this moment 3D manipulators controlled by means of end-effector position feedback are economically not feasible. However, the cost of digital image processing is decreasing, and in the future it is to be expected that this measurement technique will be applied more and more in manipulator controllers with end-effector feedback.

References

Burr Brown Corporation. 1987. *The Handbook of Linear IC Applications*. Tucson, AZ.

van Driel, M. A. M. 1988. Design of an opto-electronic tracking system for 2D measurement. (In Dutch). Report WFW 88.006. The Netherlands: Eindhoven University Press.

Heeren, T. A. G. 1989. On control of manipulators. Ph.D. thesis, Eindhoven University of Technology, The Netherlands.

Melles Griot. 1988. Optics Guide 4. Irvine, CA.

Philips Gloeilampen BV. 1988. Philips Data Handbook (Semiconductor lasers). Eindhoven, The Netherlands.